Quantum Brayton Refrigeration Cycle with Finite-Size Bose–Einstein Condensates

Jiehong Yuan(袁结红)[1], Huilin Ruan(阮慧琳)[1], Dehua Liu(刘德华)[1], Jizhou He(何济洲)[1], and Jianhui Wang(王建辉)[1,2*]

[1]*Department of Physics, Nanchang University, Nanchang 330031, China*
[2]*State Key Laboratory of Surface Physics, and Department of Physics, Fudan University, Shanghai 200433, China*

(Received 27 July 2023; accepted manuscript online 6 September 2023)

We consider a quantum Brayton refrigeration cycle consisting of two isobaric and two adiabatic processes, using an ideal Bose gas of finite particles confined in a harmonic trap as its working substance. Quite generally, such a machine falls into three different cases, classified as the condensed region, non-condensed phase, and regime across the critical point. When the refrigerator works near the critical region, both figure of merit and cooling load are significantly improved due to the singular behavior of the specific heat, and the coefficient of performance at maximum figure of merit is much larger than the Curzon–Ahlborn value. With the machine in the non-condensed regime, the coefficient of performance for maximum figure of merit agrees well with the Curzon–Ahlborn value.

DOI: 10.1088/0256-307X/40/10/100502

Like classical thermal machines, quantum heat engines and refrigerators[1–7] can be various kinds of cycle models, such as the Carnot cycle, Otto cycle, Brayton cycle, and Diesel cycle. For these machines the working substance may be trapped particles,[8] two level systems,[9,10] multilevel systems,[11] or harmonic oscillators,[12–15] which obey Bose–Einstein or Fermi–Dirac statistics. The quantum effects of the working substance, such as quantum entanglement,[16–18] coherence,[19–23] correlation,[24–26] quantum measurement,[27–29] and even phase transition,[30–32] may cause the quantum thermal machines to outperform their classical counterparts.

A Bose system as the working substance provides a very appealing platform for revealing the novel performance of a quantum thermal machine because the Bose–Einstein condensation[33,34] can result in singular behaviors of physical quantities. A significant enhancement of performance was observed for quantum Otto engines with improved efficiency and power in the region near Bose–Einstein condensation.[30] In such engines, the phase-transition-enabled improvements in performance are found by assuming a fixed trapping potential to realize a thermalization process. This limitation can be overcome by exploiting other kinds of machine cycles where the external field is varying during a thermal-contact process, though it may be technically challenging. The rest of the study of quantum heat engines includes the use of Bose–Einstein condensation as the basis for heat engines acting on a quantum field working medium,[31] and quantum heat machine cycles based on spin-orbit and Zeeman-coupled Bose–Einstein condensation.[32] It is still unclear whether a Brayton cycle,[5–7] where the trapping potential must be varied during an isobaric process, can exhibit Bose–Einstein-condensation-enhanced machine performance.

In this Letter, we address the issue of the performance for quantum Brayton refrigerators, adopting an ideal Bose gas with finite particles confined in a harmonic trap as the working substance. A refrigerator is a reversed heat engine absorbing heat $Q_{\rm l}$ from a cold reservoir of low temperature $T_{\rm l}$ and releasing heat $Q_{\rm h}$ to a hot reservoir of high temperature $T_{\rm h}$. Finite particle numbers[35–38] stands for the finite-size system far away from the thermodynamic limit typical for Bose–Einstein condensation experiments. In analogy with efficiency and power output for heat engines, the coefficient of performance (COP), $\varepsilon = Q_{\rm l}/(Q_{\rm h} - Q_{\rm l})$ and figure of merit are two performance measures for the refrigerators. Here the figure of merit, $\chi = \varepsilon Q_{\rm l}/\mathcal{T}_{\rm cyc}$[39–43] (with cycle period $\mathcal{T}_{\rm cyc}$), is the trade-off objective function predicting the optimal state in consideration of both the COP and the cooling load $Q_{\rm l}$. We show that the engine working in the three regimes performs best in the region across the critical point. This region is where the working system realizes the transition from the condensed phase to the non-condensed phase during the isobaric process. In particular, we find that the COP at maximum figure of merit is not bounded by the so-called Curzon–Ahlborn (CA) value $\varepsilon_{\rm CA} = \sqrt{1+\varepsilon_{\rm C}} - 1$,[44–47] with the Carnot COP $\varepsilon_{\rm C} = T_{\rm l}/(T_{\rm h} - T_{\rm l})$. It can surpass the CA value, which, however, requires the condition that the refrigerator works across the critical region.

Let us consider a system consisting of a finite number N of non-interacting bosons confined in a three-dimensional harmonic potential, with frequencies ω_1, ω_2, and ω_3 along the x_1, x_2, and x_3 axes. In terms of the

*Corresponding author. Email: wangjianhui@ncu.edu.cn
© 2023 Chinese Physical Society and IOP Publishing Ltd

geometric mean of these frequencies, $\Omega = (\omega_1\omega_2\omega_3)^{1/3}$, within the grand-canonical-ensemble treatment, the internal energy U and the harmonic pressure $\mathcal{P}$ [48] are given by ($\hbar \equiv k_{\rm B} \equiv 1$)

$$U = 3T\Big(\frac{T}{\Omega}\Big)^3 g_4(z) + 2\gamma T\Big(\frac{T}{\Omega}\Big)^2 g_3(z), \tag{1}$$

$$\mathcal{P} = T^4 g_4(z) + \frac{2}{3}\gamma\Omega T^3 g_3(z), \tag{2}$$

where $g_n(z) = \sum_{l=1}^{\infty} z^l/l^n$ represents the Bose–Einstein function, and γ is the coefficient related to the frequency of the individual oscillators. [49,50] The fugacity z as functions of chemical potential μ, ground-sate energy ε_0, and temperature T is given by $z = e^{(\mu-\varepsilon_0)/T}$. The detailed derivation of Eqs. (1) and (2) is presented in the Supplementary Material. [51]

When the system temperature T is not larger than the critical value $T_{\rm c}^{\mathcal{P}}$, Bose–Einstein condensation occurs and the fugacity $z \to 1$ and then $g_n(1) = \zeta(n)$, with $\zeta(x)$ denoting the Riemannian zeta function. [49] In such situations, the critical temperature at constant pressure can be derived as

$$T_{\rm c}^{\mathcal{P}} = \Big(\frac{\mathcal{P}}{\Phi}\Big)^{1/4}, \tag{3}$$

with

$$\Phi \equiv \zeta(4) + \frac{2}{3}\gamma\frac{[\zeta(3)]^{4/3}}{N^{1/3}}\Big(1 - \frac{\gamma\zeta(2)}{3[\zeta(3)]^{2/3}}\frac{1}{N^{1/3}}\Big)^{-1}.$$

For given particle number N, the critical temperature $T_{\rm c}^{\mathcal{P}}$ during an isobaric stroke is dependent on pressure $\mathcal{P}$. The equation of state for the finite-size Bose system can be obtained as [51]

$$\mathcal{P}\mathcal{V} = NTF(z), \tag{4}$$

where the quantum-correction factor reads [52]

$$F(z) = \frac{\Phi/t^4}{g_3(z) + [3g_2(z)/2g_3(z)][\Phi/t^4 - g_4(z)]}, \quad T \geq T_{\rm c}^{\mathcal{P}}$$

$$F(z) = \frac{1}{9N\Phi_t^2}\frac{\Phi_t + \zeta(4)}{\zeta(3) + [3\zeta(2)/2\zeta(3)]\Phi_t} \times \Big[\frac{8\gamma^3\zeta(3)^4}{3\Phi_t} + 4\gamma^3\zeta(2)[\zeta(3)]^2\Big], \quad T < T_{\rm c}^{\mathcal{P}} \tag{5}$$

$t = T/T_{\rm c}^{\mathcal{P}}$ is the reduced temperature [36] and $\Phi_t \equiv \Phi/t^4 - \zeta(4)$. The correction factor (5) implies $z = z(T, \mathcal{P}, N)$, which, for the given particle number N, means that $F(z) = F(T, \mathcal{P})$. Comparison between Eqs. (1) and (2) shows that the internal energy satisfies the relation $U = 3\mathcal{P}\mathcal{V}$, [52] where we have used $\mathcal{V} = \Omega^{-3}$ to indicate the so-called harmonic volume. [48] The enthalpy $\mathcal{H}$ of the ideal Bose system then reads

$$\mathcal{H} = U + \mathcal{P}\mathcal{V} = 4\mathcal{P}\mathcal{V}. \tag{6}$$

Now we are in a position to discuss the performance of a Brayton cycle alternately driven by a hot and a cold heat reservoir with temperatures $T_{\rm h}$ and $T_{\rm l}(< T_{\rm h})$, as shown in Fig. 1. This machine works with the finite-size Bose system and consists of two isobaric and two adiabatic processes. These strokes are described as follows: $1 \to 2$ ($3 \to 4$) denotes the isentropic compression (expansion), in which the working system is isolated from these two heat reservoirs. Given a trapping potential, the adiabatic formation of Bose–Einstein condensation cannot be realized due to constant fugacity z and constant ratio Ω/T. [51] Here, $2 \to 3$ ($4 \to 1$) represents an isobaric compression (expansion) with constant pressure $\mathcal{P}_{\rm h}$ ($\mathcal{P}_{\rm l}$), where the working system is weakly coupled to the hot (cold) reservoir. The system relaxes to the thermal equilibrium with the hot and cold reservoirs at the ending instants (1 and 3) of the two-thermal contacts, respectively.

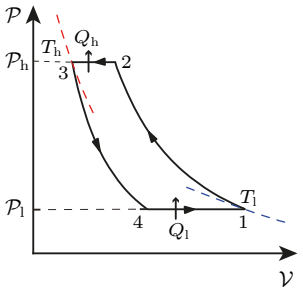

Fig. 1. Schematic diagram of the Brayton refrigeration cycle in the plane of harmonic pressure ($\mathcal{P}$) and harmonic volume ($\mathcal{V}$).

During an isobaric process, the heat exchanged between the system and the heat reservoir is determined by $\delta Q = C_{\mathcal{P}}dT$, with $C_{\mathcal{P}} = d\mathcal{H}/dT$. It follows that, using Eq. (6), the respective amounts of heat exchanged along the hot isobaric and cold isobaric processes are given by

$$Q_{\rm h} = 4\mathcal{P}_{\rm h}(\mathcal{V}_2 - \mathcal{V}_{\rm h}), \quad Q_{\rm l} = 4\mathcal{P}_{\rm l}(\mathcal{V}_1 - \mathcal{V}_4). \tag{7}$$

For each cycle, no heat is exchanged during two adiabatic processes, and thus the total work extraction is obtained as $W = Q_{\rm h} - Q_{\rm l}$. Since the entropy is kept to be constant during the two adiabatic strokes of the Brayton cycle, the COP can be written as [51] $\varepsilon = Q_{\rm l}/W = [(\mathcal{P}_{\rm h}/\mathcal{P}_{\rm l})^{1/4} - 1]^{-1}$. This expression is applicable to the ideal gas at any finite temperatures, irrespective of the presence of Bose–Einstein condensation. It follows from the fact that the formation of Bose–Einstein condensation does not change the expressions of heats as given by Eq. (7). This COP is identical to that obtained from the classical Brayton refrigeration cycle. [53,54] However, our result is obtained in a broader context by including the effects of quantum statistics, and it holds even in the case that Bose–Einstein condensation occurs.

With the relation $T_{\rm c}^{\mathcal{P}_{\rm h}}/T_{\rm c}^{\mathcal{P}_{\rm l}} = (\mathcal{P}_{\rm h}/\mathcal{P}_{\rm l})^{1/4}$ derived from Eq. (3), the COP can be re-expressed in terms of the Carnot COP and the reduced temperatures ($t_{\rm l} = T_{\rm l}/T_{\rm c}^{\mathcal{P}_{\rm l}}$ and $t_{\rm h} = T_{\rm h}/T_{\rm c}^{\mathcal{P}_{\rm h}}$):

$$\varepsilon = \frac{1}{[(\varepsilon_{\rm C}+1)/\varepsilon_{\rm C}](t_{\rm l}/t_{\rm h}) - 1}. \tag{8}$$

The expressions for heat exchanged during the hot and cold isobars can also be re-expressed by Eq. (3) and the

isobaric condition as

$$Q_{\rm h} = \frac{T_{\rm h}}{t_{\rm h}} \int_{t_{\rm h}}^{t_{\rm l}} C_{\mathcal{P}} dt, \quad Q_{\rm l} = \frac{T_{\rm l}}{t_{\rm l}} \int_{t_{\rm h}}^{t_{\rm l}} C_{\mathcal{P}} dt, \tag{9}$$

where $t_2 = t_{\rm l}$, $t_4 = t_{\rm h}$, and $C_{\mathcal{P}}$ is a function of the number of particles N and the reduced temperature t.[51] The figure of merit $\chi = \varepsilon Q_{\rm l}/\mathcal{T}_{\rm cyc}$ [39–42] with total cycle time $\mathcal{T}_{\rm cyc}$ can thus be determined by combining Eqs. (8) and (9). For our model, we assume the refrigeration cycle to be quasistatic and thus set $\mathcal{T}_{\rm cyc} = $ const. for simplicity; we focus on the isotropic harmonic trap in which the parameter γ in Eq. (1) is $\gamma = 3/2$.[49]

We plot the exact numerical solution of the figure of merit $\chi = \varepsilon Q_{\rm l}$ as functions of $t_{\rm h}$ and $t_{\rm l}$ in Fig. 2. The condition of $t_{\rm h} < t_{\rm l}$ should always be satisfied in order for the machine to operate as a refrigerator ($\chi > 0$), as shown in Fig. 2. The refrigerator may operate in three regimes: a full condensate regime where $T < T_{\rm c}^{\mathcal{P}}$, a region across the critical point where T is close to $T_{\rm c}^{\mathcal{P}}$, and a complete non-condensate case with $T > T_{\rm c}^{\mathcal{P}}$. We observe that, when $0.78 \lesssim t_{\rm h} \lesssim 0.98$ and $1.01 \lesssim t_{\rm l} \lesssim 1.23$, the figure of merit is larger. That is, the exhibition of a phase transition between condensed and non-condensed phases during a machine cycle can lead to significant enhancement of the figure of merit χ. By contrast, the machine working either in the condensed phase when $t_{\rm l,h} < 1$ or in the non-condensed phase with $t_{\rm l,h} > 1$ shows lower performance due to smaller figure of merit.

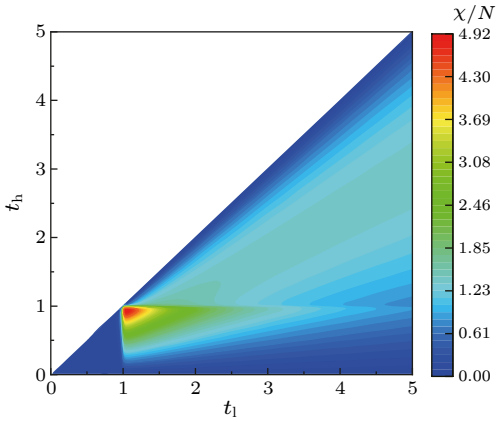

Fig. 2. Contour plot of χ/N as a function of dimensionless temperatures $t_{\rm l}$ and $t_{\rm h}$ for the trapped Bose gas with particle number $N = 200$. The parameters are $T_{\rm h} = 4$ and $T_{\rm l} = 2$.

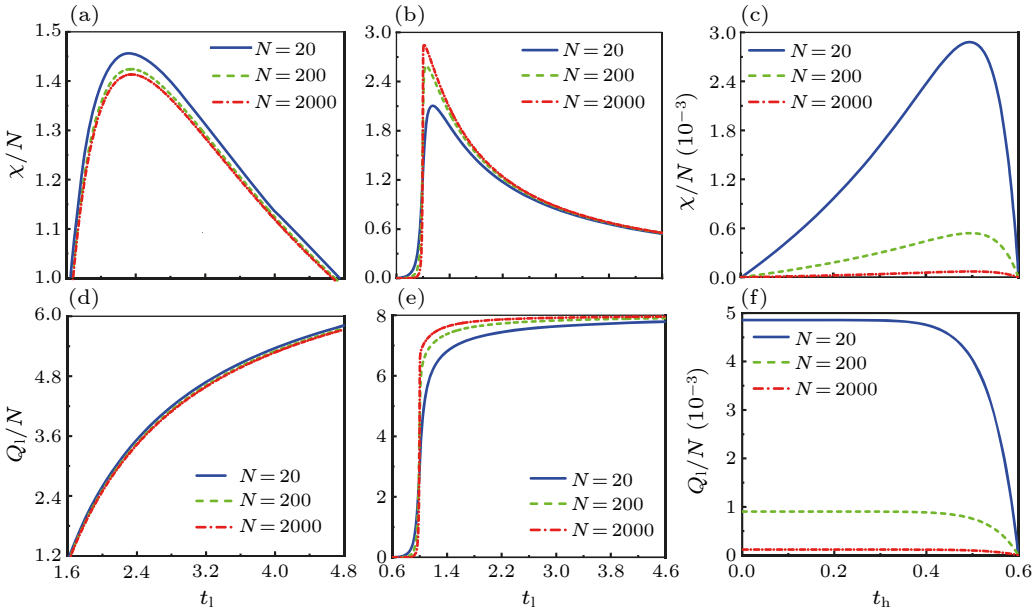

Fig. 3. Results for the refrigeration cycle with different particles in three different cases: [(a), (b)] χ/N as a function of $t_{\rm l}$ (a) when the cycle operates fully in the non-condensate phase and (b) when the cycle works across the critical region; (c) χ/N as a function of $t_{\rm h}$ for the machine working completely in the condensate phase; [(d), (e)] $Q_{\rm l}/N$ as a function of $t_{\rm l}$ (d) in the non-condensate phase and (e) in the regime across the critical point; (f) $Q_{\rm l}/N$ as a function of $t_{\rm h}$ in the condensate phase. The choices of reduced temperatures are $t_{\rm h} = 1.4$, $t_{\rm h} = 0.6$, and $t_{\rm l} = 0.6$, respectively. The temperatures $T_{\rm h}$ and $T_{\rm l}$ are the same as those in Fig. 2.

The figure of merit for the machine working in these three regions is illustrated in Figs. 3(a), 3(b), and 3(c). For the refrigerator working either in the condensate region or in the non-condensed phase, the figure of merit per particle χ/N decreases with increasing particle number N, as shown in Figs. 3(a) and 3(c). By contrast, the figure of merit per particle χ/N for the machine operating with phase transition increases with increasing particle number N [cf. Fig. 3(b)].

The difference of the figure of merit in Figs. 3(a), 3(b), and 3(c) can be physically explained by the behavior of the specific heat associated with heat injection $Q_{\rm l}$. We examine the specific heat of a trapped ideal Bose gas with finite particle number N, and show that the critical behavior

at the Bose–Einstein condensation is revealed by a sharp cusp of the specific heat, and that the specific heat in the condensed phase is smaller than that in the non-condensed region.[51] For a low heat capacity, a small amount of heat is required to change the temperature of the system, while at a high heat capacity the system will require more energy to change the temperature by the same amount. Therefore, the heat injection $Q_{\rm l}$ is relatively small in the condensed phase where $C_{\mathcal{P}}$ is quite low, as shown in Fig. 3(f). Comparing this with Figs. 3(d) and 3(e), we observe that the heat $Q_{\rm l}$ is thus much smaller in the condensed phase than those in the out-of-condensed case and in the region across the critical point, as it should be. When the machine operates across the critical region, $Q_{\rm l}$ has the largest values owing to the cusp-type behavior of the heat capacity near the phase transition point. In stark contrast to both full condensate and non-condensate regimes where specific heat decreases with increasing particle number N, in the regime near the transition point the specific heat per particle increases with increasing N. This results in the fact that, in contrast to the full condensate and non-condensate cases, both figure of merit per particle χ/N and cooling load $Q_{\rm l}/N$ increase with increasing N when the machine works across the critical point.

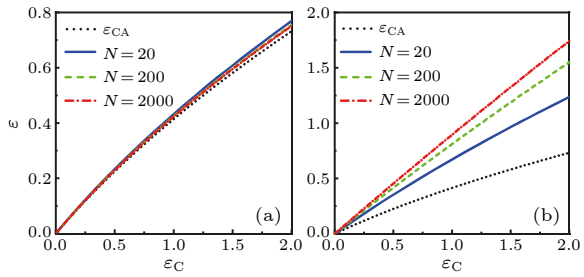

Fig. 4. COP ε at maximum figure of merit χ as a function of the Carnot COP $\varepsilon_{\rm C}$ in two cases, for different values of particle numbers N. (a) The numerical results for the entire cycle in the non-condensed phase, where $t_{\rm h}=1.4$. (b) The numerical results for the global region of the entire cycle across the critical point. Parameters are the same as those in Fig. 2.

Since the figure of merit of a refrigerator vanishes at maximum COP, the COP at maximum figure of merit is the machine measure of significance for practical applications. We maximize the figure of merit with respect to the ratios $t_{\rm h}$ and $t_{\rm l}$, by keeping all other parameters, such as temperatures $T_{\rm h,l}$ and cycle time $\mathcal{T}_{\rm cyc}$, being constant. In view of the fact that both cooling load and figure of merit are particularly small in the condensed phase, the optimal analysis is presented only in the two cases: the engine works across the critical region and it operates in the non-condensed region. By properly adjusting the parameters $t_{\rm h}$ and $t_{\rm l}$ to satisfy the optimal condition of maximal χ, the refrigerator working in the region that crosses the critical point has an optimal COP much larger than the CA COP $\varepsilon_{\rm CA}$, and in the non-condensed case it operates at the optimized COP in good agreement with the CA value [see Figs. 4(a) and 4(b)]. Unlike in the case far away from the critical point, the COP at maximum figure of merit near the critical point increases with increasing particle number N, due to the cooling load per particle (in Fig. 3) which can be enhanced by increasing the system size.

According to Eq. (4), the isobaric process can reach

$$\frac{T_2}{T_{\rm h}}=\frac{\mathcal{V}_2F(T_{\rm h},\mathcal{P}_{\rm h})}{\mathcal{V}_{\rm h}F(T_{\rm l},\mathcal{P}_{\rm l})},\quad \frac{T_4}{T_{\rm l}}=\frac{\mathcal{V}_4F(T_{\rm l},\mathcal{P}_{\rm l})}{\mathcal{V}_{\rm l}F(T_{\rm h},\mathcal{P}_{\rm h})},$$

and we use Eq. (7) to re-express the cooling load as

$$Q_{\rm l}=4NkT_{\rm l}F(T_{\rm l},\mathcal{P}_{\rm l})\Big[1-\frac{F(T_{\rm h},\mathcal{P}_{\rm h})t_{\rm h}}{F(T_{\rm l},\mathcal{P}_{\rm l})t_{\rm l}}\Big]. \tag{10}$$

In the high-temperature limit[55] where the quantum effects are vanishing, the quantum-correction factor in state function (4) approaches 1, which means that $F(T_{\rm h},\mathcal{P}_{\rm h})\approx F(T_{\rm l},\mathcal{P}_{\rm l})\approx 1$. In such a situation, the cooling load (10) simplifies to $Q_{\rm l}=4NT_{\rm l}(1-t_{\rm h}/t_{\rm l})$, yielding

$$\chi=\frac{4NT_{\rm l}(1-t_{\rm h}/t_{\rm l})}{[(\varepsilon_{\rm C}+1)/\varepsilon_{\rm C}](t_{\rm l}/t_{\rm h})-1}.$$

By setting $\partial\chi/\partial t_{\rm h}=0$ and $\partial\chi/\partial t_{\rm l}=0$, we have

$$\frac{t_{\rm l}}{t_{\rm h}}=\frac{(1+\varepsilon_{\rm C}+\sqrt{1+\varepsilon_{\rm C}})}{(1+\varepsilon_{\rm C})}.$$

Substituting this optimality relation into Eq. (8), we reproduce the CA COP, namely, $\varepsilon^*=\varepsilon_{\rm CA}=\sqrt{\varepsilon_{\rm C}+1}-1$, as is expected.

In summary, we have theoretically proposed a Brayton refrigerator model that uses an ideal gas with a finite number of particles confined in a three-dimensional harmonic trap as its working substance. It is shown that the engine working in the region across the Bose–Einstein-condensation transition point can outperform its non-transition counterpart by dramatically enhancing figure of merit χ and cooling load $Q_{\rm l}$. While the COP at maximum figure merit agrees well with the CA COP when no Bose–Einstein condensation occurs during the cycle, it can beat the CA value when the machine cycle works across the critical point. Our findings demonstrate the potential of quantum engines utilizing phase transition and singularity of physical quantities to realize ideal thermal machines with an overall good performance.

Acknowledgments. This work was supported by the National Natural Science Foundation of China (Grant No. 11875034), and the Major Program of Jiangxi Provincial Natural Science Foundation (Grant No. 20224ACB201007). J. W. also acknowledges financial support from the Opening Project of Shanghai Key Laboratory of Special Artificial Microstructure Materials and Technology.

References

[1] Wang L Q, Wang Z, Wang C, and Ren J 2022 *Phys. Rev. Lett.* **128** 067701
[2] Wang Y and Tu Z C 2012 *Phys. Rev. E* **85** 011127
[3] Chen J F, Sun C P, and Dong H 2019 *Phys. Rev. E* **100** 032144
[4] Zhang Y C and He J Z 2013 *Chin. Phys. Lett.* **30** 010501
[5] Saygın H and Şişman A 2001 *Appl. Energy* **69** 77

[6] Lin B H and Chen J C 2003 *Phys. Rev. E* **68** 056117
[7] He J Z, Xin Y, and He X 2007 *Appl. Energy* **84** 176
[8] Bener C M, Brody D C, and Meister B K 2000 *J. Phys. A* **33** 4427
[9] Leggio B and Antezza M 2016 *Phys. Rev. E* **93** 022122
[10] Erdman P A, Cavina V, Fazio R, Taddei F, and Giovannetti V 2019 *New J. Phys.* **21** 103049
[11] Quan H T, Zhang P, and Sun C P 2005 *Phys. Rev. E* **72** 056110
[12] Kosloff R and Rezek Y 2017 *Entropy* **19** 136
[13] Reid B, Pigeon S, Antezza M, and de Chiara G 2017 *Europhys. Lett.* **120** 60006
[14] Abah O and Lutz E 2016 *Europhys. Lett.* **113** 60002
[15] Frim A G and DeWeese M R 2022 *Phys. Rev. E* **105** L052103
[16] Zhang T, Liu W T, Chen P X, and Li C Z 2007 *Phys. Rev. A* **75** 062102
[17] Funo K, Watanabe Y, and Ueda M 2013 *Phys. Rev. A* **88** 052319
[18] Ji Y H, Hu J J, and Hu Y 2012 *Chin. Phys. B* **21** 110304
[19] Francica G, Goold J, and Plastina F 2019 *Phys. Rev. E* **99** 042105
[20] Camati P A, Santos J F G, and Serra R M 2019 *Phys. Rev. A* **99** 062103
[21] Rahav S, Harbola U, and Mukamel S 2012 *Phys. Rev. A* **86** 043843
[22] Wen J and Li G Q 2018 *Chin. Phys. Lett.* **35** 060301
[23] Brandner K, Bauer M, and Seifert U 2017 *Phys. Rev. Lett.* **119** 170602
[24] Yang Y Y, Li L J, Ye L, and Wang D 2022 *Chin. Phys. B* **31** 100303
[25] Wang C and Chen Q H 2013 *New J. Phys.* **15** 103020
[26] Fei Z Y, Quan H T, and Liu F 2018 *Phys. Rev. E* **98** 012132
[27] Horowitz J M and Jacobs K 2014 *Phys. Rev. E* **89** 042134
[28] Lin Z Y, Su S H, Chen J Y, Chen J C, and Santos J F G 2021 *Phys. Rev. A* **104** 062210
[29] Chand S, Dasgupta S, and Biswas A 2021 *Phys. Rev. E* **103** 032144
[30] Myers N M, Peña F J, Negrete O, Vargas P, Chiara G D, and Deffner S 2022 *New J. Phys.* **24** 025001
[31] Gluza M, Sabino J, Ng N H Y, Vitagliano G, Pezzutto M, Omar Y, Mazets I, Huber M, Schmiedmayer J, and Eisert J 2021 *PRX Quantum* **2** 030310
[32] Li J, Sherman E Y, and Ruschhaupt A 2022 *Phys. Rev. A* **106** L030201
[33] Anderson M H, Ensher J R, Matthews M R, Wieman C E, and Cornell E A 1995 *Science* **269** 198
[34] Li Z, Wang J Z, and Fu L B 2013 *Chin. Phys. Lett.* **30** 010301
[35] Dai W S and Xie M 2004 *Phys. Rev. E* **70** 016103
[36] Wang J H and Mang Y L 2010 *J. Phys. B* **43** 175301
[37] Jiang J H, Entin-Wohlman O, and Imry Y 2012 *Phys. Rev. B* **85** 075412
[38] Su G Z, Chen L W, and Chen J C 2014 *Phys. Lett. A* **378** 1992
[39] Izumida Y, Okuda K, Hernández A C, and Roco J M M 2013 *Europhys. Lett.* **101** 10005
[40] Allahverdyan A E, Hovhannisyan K, and Mahler G 2010 *Phys. Rev. E* **81** 051129
[41] Wang Y, Li M, Tu Z C, Hernández A C, and Roco J M M 2012 *Phys. Rev. E* **86** 011127
[42] Hu Y, Wu F, Ma Y, He J, Wang J, Hernández A C, and Roco J M M 2013 *Phys. Rev. E* **88** 062115
[43] Hernández A C, Medina A, and Roco J M M 2015 *New J. Phys.* **17** 070511
[44] Curzon F L and Ahlborn B 1975 *Am. J. Phys.* **43** 22
[45] Luo X G, Liu N, and He J Z 2013 *Phys. Rev. E* **87** 022139
[46] Liu H G, He J Z, Wang J H 2023 *Chin. Phys. B* **32** 030503
[47] Yuan Y, Wang R, He J Z, Ma Y L, and Wang J H 2014 *Phys. Rev. E* **90** 052151
[48] Romero-Rochín V 2005 *Phys. Rev. Lett.* **94** 130601
[49] Grossmann S and Holthaus M 1995 *Z. Naturforsch. A* **50** 921
[50] Grossmann S and Holthaus M 1995 *Phys. Lett. A* **208** 188
[51] See the Supplemental Material for the detailed derivations of main-text equations and supplemental evidence.
[52] Pathria R K and Beale P D 2011 *Statistical Mechanics* 3rd edn (New York: Academic)
[53] Quan H T 2009 *Phys. Rev. E* **79** 041129
[54] Perrot P 1998 *A to Z of Thermodynamics* (Oxford: Oxford University Press)
[55] Galve F, Pachon L A, and Zueco D 2010 *Phys. Rev. Lett.* **105** 180501